Remote Sensing of Environment 204 (2018) 229–243

Contents lists available at ScienceDirect

Remote Sensing of Environment

journal homepage: www.elsevier.com/locate/rse

Validating modeled lidar waveforms in forest canopies with airborne laser scanning data

Wenge Ni-Meister[a,*], Wenze Yang[b], Shihyan Lee[c], Alan H. Strahler[d], Feng Zhao[e]

[a] Department of Geography, Hunter College of The City University of New York, New York, NY, United States
[b] ESSIC, The University of Maryland at College Park, MD, United States
[c] SAIC/NASA Ocean Biology, Goddard Space Flight Center, Greenbelt, MD, United States
[d] Department Earth and Environment, Boston University, Boston, MA, United States
[e] Department of Geographical Sciences, University of Maryland, College Park, MD, United States

ARTICLE INFO

Keywords:
Lidar waveform modeling
Analytical Clumped Two-Stream (ACTS) model of canopy radiative transfer
Model validation

ABSTRACT

A thorough evaluation of the capability of modeling vegetation lidar returns is a critical aspect of deriving vegetation structure from lidar measurements. This study assesses the performance of the Analytical Clumped Two-Stream (ACTS) canopy radiative transfer model to simulate large-footprint lidar waveforms. Modeled lidar waveforms were compared to airborne Laser Vegetation Imaging Sensor (LVIS) data collected in deciduous and conifer forests: Harvard Forest, MA; Bartlett Experimental Forest, NH; and Howland Experimental Forest, ME. The simulated and LVIS lidar waveforms have coefficients of determination $R^2 > 0.9$ and RMSE ~ 0.01 at both plot and stand level for most sites. The ACTS model also produces realistic multi-peak returns from vegetation for the multi-layer and multi-species canopies with $R^2 \sim 0.79$–0.86 and RMSE ~ 0.01 between the simulated and LVIS waveforms. This validation work lays the foundation to retrieve vegetation structure and above-ground biomass directly from lidar waveforms through model inversion with the ACTS model.

1. Introduction

Vegetation structure plays a critical role in ecosystem processes, habitat and biodiversity (Spies, 1998). Vertical foliage distribution controls the amount of radiation absorbed by vegetation for photosynthesis and conductance and is linked to wildlife habitats and species diversity (Goetz et al., 2007). Horizontal distribution of canopy elements and gaps aids tree regeneration and understory development. Crown shape and size distribution and densities are indicators of tree age distributions and are related to vegetation growth and nest site availability.

Over the last decade an advanced mechanistic model of forest ecosystem dynamics has been developed to use explicit ecosystem composition and structure to link ecosystem processes and functions (Moorcroft et al., 2001). The Ecosystem Demography Biosphere (ED) model of Moorcroft et al. (2001) took a tree size- and patch age-structured approach to represent vegetation horizontal and vertical heterogeneity for vegetation dynamics. Ent (Kiang et al., 2008) is the first dynamic global terrestrial ecosystem model (DGTEM) to take the size- and age-structured approach of ED to the global scale for coupling with atmospheric general circulation models (AGCMs). As an advance over ED, the Ent DGTEM introduces a canopy radiative transfer submodel, the Analytical Clumped Two-Stream (ACTS) model (Ni-Meister et al., 2010a; Yang et al., 2010) to calculate radiation absorption, photosynthesis, conductance and energy balance. For these structure-based DGVM models, structure parameters such as vegetation height, crown size, density, and vertical foliage density are the drivers for terrestrial ecosystem carbon stocks and fluxes estimates. Correct initialization of vegetation structure inputs for these models is critical for improved estimates of global vegetation carbon storage and fluxes.

Vegetation structures can be obtained through several types of measurements, such as in-situ field measurements and remote sensing measurements including optical, radar and lidar. Field measurements of vegetation structure are time consuming, difficult to obtain, and it is impossible to get global coverage. Conventional optical and radar remote sensing may suffer from saturation problems and shading effect on satellite signals (Ni-Meister, 2015). In contrast, lidar directly measures horizontal and vertical vegetation structure of ecosystems (Dubayah and Drake, 2000). It has been recognized as the state-of-the-art remote sensing technology for mapping vegetation structure characteristics and aboveground biomass (AGB).

Recently, large amount lidar data ranging from large footprint (footprint size ≥ 10 m) and small footprint (footprint size < 10 m) have become more widely available to study vegetation structure

* Corresponding author at: Department of Geography, Hunter College of the City University of New York, 695 Park Ave., New York, NY 10065, United States.
E-mail address: Wenge.Ni-Meister@hunter.cuny.edu (W. Ni-Meister).

http://dx.doi.org/10.1016/j.rse.2017.10.028
Received 25 February 2017; Received in revised form 12 October 2017; Accepted 17 October 2017
Available online 06 November 2017
0034-4257/

Nomenclature

Roman alphabet

$B(\xi)$	volume scattering phase function of plant canopies
b	vertical crown radius
$f_1(t)$	temporal distribution of lidar pulse
$f_2(x,y)$	spatial distribution of lidar energy within a footprint
$G(\theta)$	leaf orientation function
h_c	crown center height
h_1	the lower bound of canopy height
h_2	the upper bound of canopy height
J_0	beam irradiance of the lidar
$L(z)$	accumulated leaf area index from canopy top to height z
L_t	total leaf area index
$L_e(z.\theta)$	effective LAI at height, z and beam incident zenith angle, θ
$P(\theta, z)$	canopy gap probability at height, z and beam zenith angle, θ
$P(z)$	canopy gap probability at height, z for nadir pointing laser beam
P	horizontal crown radius
$R_v(z)$	accumulated laser energy return from the canopy top to height z
R_g	laser energy return from the ground
R_{v1} and R_{v2}	accumulated laser returns from canopy for two adjacent lidar waveforms
R_{g1} and R_{g2}	laser returns of background for two adjacent lidar waveforms.
R^2	coefficient of determination
r_L	leaf reflectance
t_L	leaf transmittance
z	height in the canopy

Greek alphabet

λ	stem count density
$\gamma(\theta)$	clumping factor
ρ_v	volume backscattering coefficient of a canopy element
ρ_g	backscattering coefficient of the ground
θ	beam zenith angle
τ	light attenuation factor in canopy *(1/m)*
ω	single scattering albedo of leaf and $\omega = r + t$

Acronyms and definitions

AGB	above ground biomass
ACTS	Analytical Clumped Two-Stream
DGTEM	dynamic global terrestrial ecosystem model
Ent-DGTEM	Ent dynamic global terrestrial ecosystem model
GCM	Global atmospheric Circulation Model
GLAS	Geoscience Laser Altimeter System
GORT	geometric optical and radiative transfer
HAG-LAI	LAI based on the ground lidar hinge angle measurements
HEM-LAI	LAI from digital hemispherical photography
ICESat	Cloud, and land Elevation Satellite
LAI	leaf area index
LIC-LAI	LAI using the LAI-2000 Plant Canopy Analyzer (Lic-2000)
LVIS	land, vegetation, and ice sensor (LVIS)
PAR	photosynthetically active radiation
REG-LAI	LAI from regression of multiple angles ground lidar measurements
RH25	relative height (RH) to the ground elevation at which 25% of the accumulated full-waveform energy occurs
RH50	relative height (RH) to the ground elevation at which 50% of the accumulated full-waveform energy occurs
RH75	relative height (RH) to the ground elevation at which 75% of the accumulated full-waveform energy occurs
RH100	relative height (RH) to the ground elevation at which 100% of the accumulated full-waveform energy occurs
RMSE	root-mean-square-error
SLICER	Scanning lidar Imager of Canopies by Echo Recovery

characteristics. Full waveform large footprint lidar data are available at global and regional scales. The spaceborne Geoscience Laser Altimeter System (GLAS), part of the Ice, Cloud, and land Elevation Satellite (ICESat) mission, provided global LiDAR data with a variable diameter ~ 70 m footprint spaced at ~170 m from 2003 to 2009 (Zwally et al., 2002; Harding and Carabajal, 2005; Lefsky et al., 2005). Airborne full waveform data have also been collected using a Scanning Lidar Imager of Canopies by Echo Recovery (SLICER) with a 15 m footprint and by the Laser Vegetation Imaging Sensor (LVIS) with a 10–25 m footprint over several large areas for improved vegetation structure characterization (Blair et al., 1999). The future Global Ecosystems Dynamics Investigation Lidar (GEDI) mission will provide unique 3-D views of global vegetation structure for global carbon studies at 25 m footprint level. Small-footprint full waveform lidar data are now used at the operational level in forest resource inventories (Hancock et al., 2017). Even ground-based waveform lidar systems are available to measure complex and detailed vegetation structure over various study sites (Jupp et al., 2009; Strahler et al., 2008). These global and regional waveform lidar data provide detailed vegetation structure and biomass maps necessary for terrestrial ecosystem models and global carbon balance studies.

Waveform lidar continuously records the signal of the laser pulse as it penetrates through the plant canopy, resulting in complete vertical vegetation profiles. It has the potential to provide much richer 3D canopy characteristics than discrete lidar (Hancock et al., 2015, 2017) to study ecosystem processes and biological diversity. Both spaceborne and airborne waveform lidar has been successfully used to map vegetation height and AGB (Drake et al., 2002a, 2002b, 2003; Lefsky et al., 1999, 2002, 2005; Ni-Meister et al., 2010b; Rosette et al., 2008).

To fully understand the relationship between vegetation structure details and lidar waveforms, many canopy radiative transfer models have been adopted to simulate lidar waveforms. For example, Monte-Carlo ray-tracing based lidar models have been used to simulate lidar waveforms (Gastellu-Etchegorry et al., 2016; Disney et al., 2010; Sun and Ranson, 2000; Calders et al., 2013; North et al., 2010). These models have been used to assess sensor acquisition properties, their sensitivity to site-specific conditions and vegetation structure accuracy (Rosette et al., 2013; Hancock et al., 2008). Some have been inverted to retrieve vegetation structure parameters (Bye et al., 2017).

Analytical models have also been used for lidar waveform modeling (Sun and Ranson, 2000; Ni-Meister et al., 2001). The Geometric Optical-Radiative Transfer (GORT) model was developed to describe the interaction of three-dimensional canopy structure with the radiation environment at the forest stand scale through merging theories from geometric optics and radiative transfer (Li et al., 1995). GORT has been successfully applied to model airborne and below-canopy vegetation lidar waveforms as a function of vegetation structure parameters such as tree size, height, stem county density, and foliage volume density (Ni-Meister et al., 2001, 2008). These types of models provide computationally efficient estimations of waveforms.

More recently, we developed a simplified GORT - Analytical Clumped Two-Stream (ACTS) model through fusion of a two-stream scheme with geometric optical theory to account for the effect of hierarchical foliage clumping due to heterogeneous vegetation

structure on the light environment in vegetation canopies (Ni-Meister et al., 2010a and Yang et al., 2010). Currently, ACTS is incorporated into the Ent Dynamic Global Terrestrial Ecosystem Model (Ent-DGTEM), which is imbedded in the current NASA Global Atmospheric Circulation Models (GCMs).

New additions in ACTS include the woody component of vegetation structure to model the interaction of ground-based lidar with vegetation structure. It also deals with mixed and multilayer forests (Ni-Meister et al., 2010a). Yang et al. (2011) extended ACTS to simulate lidar waveforms, especially to study the impact of surface topography and footprint size on waveforms. This scheme was used to retrieve vegetation height from ICESat measurements over sloping terrains with good accuracy in deciduous forests in White Mountain, NH, and boreal forests in Alaska (Lee et al., 2011 and Selkowitz et al., 2012). This model was also used to extract canopy gap fraction (Armston et al., 2013; Chen et al., 2014) and to retrieve vertical foliage profiles from waveform lidar (Tang et al., 2012, 2014). All these results suggest that ACTS is a powerful tool to study the relationships between vegetation structure and waveform lidar returns.

The simple ACTS model was designed to describe averaged radiation regime within plant canopies at the tree stand scale. They are particularly well suited to study large-footprint lidar observations and small footprint lidar integrated at plot levels. The inputs are distribution functions of tree geometry parameters (such as mean tree size, shape and density) within stands/plots and the spectral properties of canopy elements and background. These simple models will provide unique advantages when used in inversion studies.

For ACTS to be fully valuable for inversion, a complete evaluation of the forward ACTS model is required. The purpose of this study is to use ACTS to simulate lidar waveforms and evaluate the capability of modeling vegetation lidar returns. The paper is organized as following: Section 2 describes the ACTS model in detail. Sections 3 and 4 include validation sites, field measurements, lidar data and model inputs. Section 5 discusses the evaluation results, and Section 6 has the conclusions. In Section 7, we point out recent and potential applications of the ACTS model.

2. The physical model

2.1. The ACTS model

Like all geometric optical models, ACTS treats vegetation canopies as assemblages of randomly distributed tree crowns of ellipsoidal shape. It allows for multi-layered and multispecies canopies (Fig. 1). It accounts for the effect of hierarchical foliage clumping due to heterogeneous vegetation structure on the light environment in vegetation canopies through fusion of a two-stream scheme with geometric optical theory (Ni-Meister et al., 2010a, 2010b; Yang et al., 2010). Compared to previous versions of the GORT model, ACTS features (1) description of horizontal heterogeneity by a clumping factor, and vertical heterogeneity by an actual foliage profile; and (2) extended multi-layer and multi-species modeling ability.

The key feature of ACTS for vegetation lidar applications lies in its ability to describe the interactions of the laser pulse with vegetation structure and its fundamental capability to model vegetation gap probability as a function of vegetation structure parameters. Canopy gap probability or uncollided transmittance is defined as the portion of photons passing through the gaps of the vegetation canopy without hitting any canopy elements. In ACTS, it is calculated as an exponential decay as a function of vertical foliage profile and a clumping factor assuming randomly distributed ellipsoid crowns in space with a limitation that they do not grow together. The expressions for the clumping factor and foliage profiles are functions of tree size, shape and density, and foliage area volume density for single layered or multi-layered canopies. Canopy gap probability, $P(\theta, z)$ with height, z, and beam zenith angle, θ is described as:

$$\begin{cases} P(\theta,z) = exp\left(\frac{-\gamma(\theta)G(\theta)L(z)}{cos(\theta)}\right) \\ \gamma(\theta) = \frac{3}{4\pi R}\left(1 - \frac{1-(2\tau R+1)e^{-2\tau R}}{2\tau^2 R^2}\right) \\ \tau R = \frac{3GL_t}{(4\lambda\pi R^2)\left(\frac{1+tan^2\theta}{1+\left(\frac{b}{R}\right)^2 tan^2\theta}\right)^2} \end{cases} \quad (1)$$

where z is the height in the canopy, $G(\theta)$ is a leaf orientation function, $L(z)$ is the accumulated leaf area index from canopy top to height z, calculated based on tree geometry inputs (Ni-Meister et al., 2001, 2010a). The factor $\gamma(\theta)$ is the clumping factor, which is a function of tree geometry inputs and laser incident zenith angle, θ. τ is the attenuation factor (m^{-1}) and L_t is the total leaf area index, and the effective LAI is $L_e(z,\theta) = L(z)\gamma(\theta)$. R and b are the horizontal and vertical crown radii. λ is the crown count density. The attenuation of light passing through a canopy or canopy gap probability is a function of the density, size and distribution (horizontal and vertical) of foliage and woody elements within the canopy. As this study deals with nadir pointing lidar, through the whole paper, $P(z)$ is used to represent gap probability for nadir pointing lidar, simply written as,

$$P(z) = \exp(-G(0)\gamma(0)L(z) = \exp(-G(0)L_e(z) \quad (2)$$

2.2. Lidar waveform modeling using ACTS

ACTS simulates lidar waveforms as a convolution of laser pulse function (using a Gaussian function for large footprint lidar, Hancock et al., 2017) and laser energy intercepted/reflected by vegetation canopy and the laser energy reflected from the background. The basic lidar equation is described as (Ni-Meister et al., 2001; Yang et al., 2011):

$$-\frac{dR_v(z)}{dz} = J_0\rho_v \int f_2(x,y)^*\left(\int f_1(t)^*\frac{dP(z)}{dz}\,dt\right)dx\,dy = J_0\rho_v\frac{dP^*(z)}{dz} \quad (3)$$

$$R_g = J_0\rho_g \int f_2(x,y)^*\left(\int f_1(t)^*P(0)\,dt\right)dx\,dy = J_0\rho_g P^*(0) \quad (4)$$

where $R_v(z)$ is the accumulated laser energy return from the canopy top to height z; R_g is the laser energy return from the ground; J_0 is the beam irradiance of the lidar; ρ_v is the volume backscattering coefficient of a canopy element; ρ_g is the backscattering coefficient of the ground; $f_1(t)$ describes the temporal distribution of lidar pulse; $f_2(x,y)$ describes the spatial distribution of lidar energy within a footprint; f_1 and f_2 are both Gaussian distributions for large footprint lidar (Hancock et al., 2017),

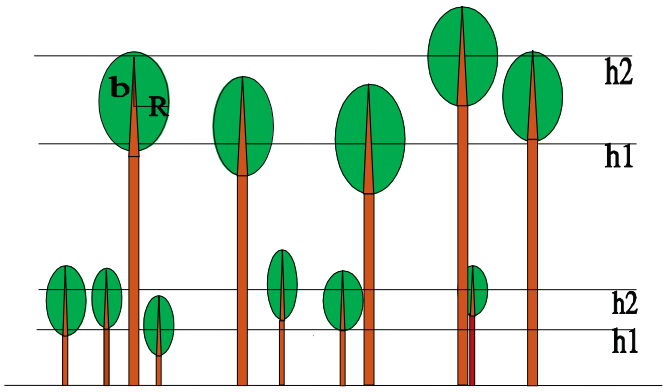

Fig. 1. Vertical cross section of a two-layer vegetation canopy scene showing the tree crown with ellipsoid shape and different size and density distributed in space, vertical and horizontal crown radii are labeled as b and r, while the height of lower and upper bounds of crown centers are labeled as h1 and h2 for both overstory and understory layers (Ni-Meister et al., 2010a).

the specific parameters depend on the lidar sensor itself; $P(z)$ is the canopy gap probability; "*" refers to convolution computation; $P^*(z)$ is the convoluted $P(z)$:

$$\frac{dP^*z)}{dz} = \int f_2(x,y)^* \left(\int f_1(t)^* \frac{dP(z)}{dz}\, dt \right) dx\, dy \tag{5}$$

$$P^*(0) = \int f_2(x,y)^* \left(\int f_1(t)^* P(0)\, dt \right) dx\, dy \tag{6}$$

As the laser energy returns are not calibrated, the original waveform usually is normalized by the total digital count,

$$\frac{-\frac{dR_v(z)}{dz}}{R_v(0)+R_g} = \frac{\frac{dP^*(z)}{dz}}{[1-P^*(0)]+\frac{\rho_g}{\rho_v}P^*(0)}$$

$$R_g = \frac{P^*(0)}{[1-P^*(0)]\frac{\rho_v}{\rho_v}+P^*(0)} \tag{7}$$

where $R_v(z)$, $R_v(0\ )$, and R_g are the laser returns from the canopy top to height z, from canopy top to ground, and from the ground return, respectively; and ρ_v/ρ_g is the ratio of the volume backscattering coefficients of the vegetation and background.

The volume backscattering coefficient of a canopy volume, ρ_v, is a function of the leaf angular distribution, the phase function of leaf scattering and the spectral properties (e.g. transmittance and reflectance). Ni-Meister et al. (2001) provides a detailed description on how to obtain ρ_v for lidar. For randomly oriented Lambertian leave

$$\rho_v = \frac{\omega}{4} B(\xi) \tag{8}$$

where ω is the single scattering albedo of the leaf and $\omega = r_L + t_L$ (r_L is the leaf reflectance and t_L is the leaf transmittance) and $B(\xi)$ is the volume scattering phase function of the plant canopy. For randomly oriented Lambertian leaves,

$$B(\xi) = \frac{8}{\omega}\left(\frac{\omega}{3\pi}(\sin\xi - \xi\cos\xi) + \frac{t}{3}\cos\xi \right) \tag{9}$$

where ξ is the scattering angle. For laser photon return at hotspot direction, $\xi = \pi$, and

$$\rho_v = \frac{2}{3} r_L \tag{10}$$

Soil is treated as a Lambertian surface and the backscattering coefficient of background is the soil albedo, ρ_g. The canopy and background reflectivity ratio then becomes

$$\frac{\rho_v}{\rho_g} = \frac{2}{3}\frac{r_L}{\rho_g} \tag{11}$$

3. Study site and data description

3.1. Study sites

The study sites include Harvard Forest in central Massachusetts, Bartlett Experimental Forest in north central New Hampshire, and Howland Ecosystem Research Forest in central Maine, as shown in Fig. 2. The sites were selected to cover regions with large spatial variations of forest types and environmental conditions.

Harvard Forest lies within the transition zone of hardwoods-white pine-hemlock, and the stands are comprised mainly of red oak (*Quercus rubra*), red maple (*Acer rubrum*), yellow birch (*Betula allleghaniensis*), white birch (*B. papyrifera*), beech (*Fagus grandifolia*), white pine (*Pinus strobus*), and hemlock (*Tsuga canadensis*). This site was designed as a Long Term Ecological Research (LTER) site in 1989 in Petersham, MA, and has been used to measure CO_2 and H_2O exchanges between the forest and atmosphere since then (Barford et al., 2001).

Bartlett Experimental Forest is located within the White Mountain National Forest, a heavily forested and mountainous region in north-central New Hampshire (Anderson et al., 2006, 2008). This site was established by the US Forest Service in 1931 for the study of secondary deciduous and coniferous forest dynamics and ecology. The major tree species in this area are American beech (*Fagus grandifolia*), red maple (*Acer rubrum*), eastern hemlock (*Tsuga canadensis*), sugar maple (*Acer saccharum*), yellow birch (*Betula alleghaniensis*), paper birch (*Betula papyrifera*), red spruce (*Picea rubens*) and balsam fir (*Abies balsamea*), with some localized small stands of eastern white pine (*Pinus strobus*).

The Forest Ecosystem Research site in Howland, ME, is located

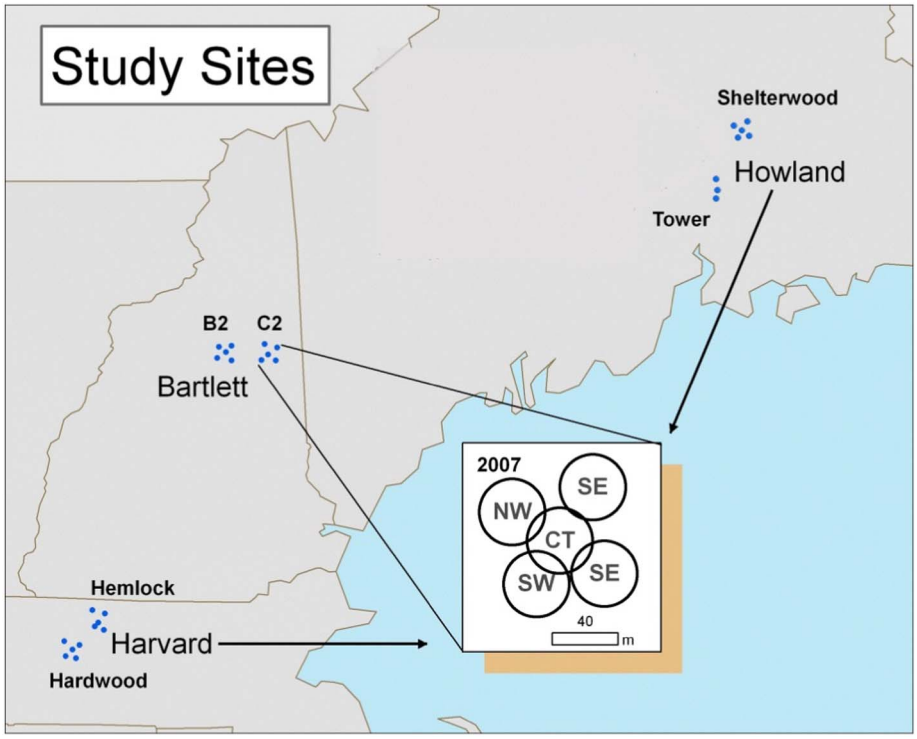

Fig. 2. Locations of our study sites (blue dots) in Harvard Forest, MA, Bartlett Experimental Forest, NH, and the Forest Ecosystem Research site in Howland, ME and sampling strategies (from Ni-Meister et al., 2010a, 2010b). Bottom right square shows the typical arrangements of plots and ranges of 2007 field data collection strategy. Five plots (NE, SW, SE, and NE are from four corners and CT from the center of the stand). The plot sizes are 20 m/25 m radius circles with 5 m geolocation accuracy. Plot centers were taken as their observed GPS coordinates; the estimated position error of the centers is about ± 1.4 m. (For interpretation of the references to color in this figure legend, the reader is referred to the web version of this article.)

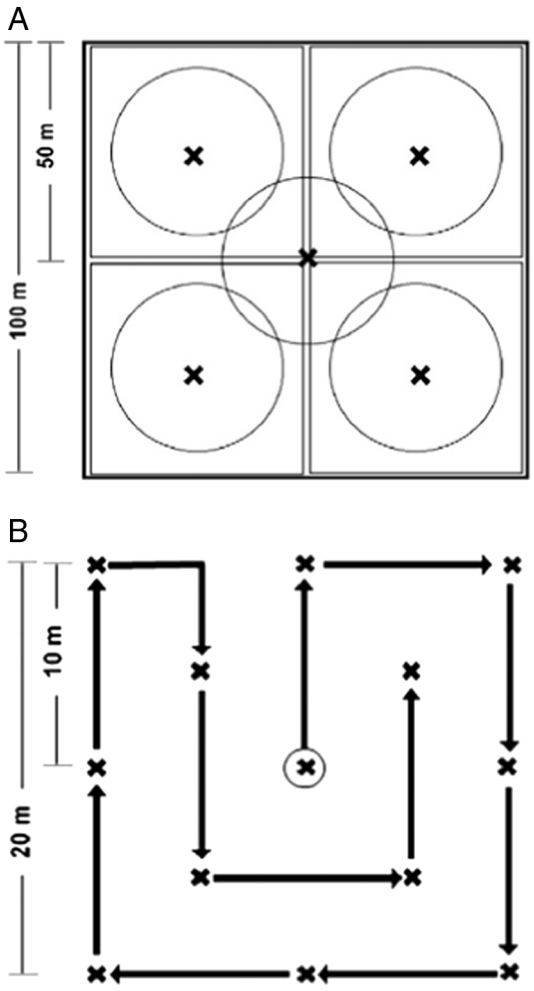

Fig. 3. Sample layout. (A) Sample layout for Echidna® ground-based lidar scans. Five scans were acquired at each site. (B) Sample layout for LAI-2000 observations and hemispherical photographs. At each scan point, 13 LAI-2000 and hemispherical photo measurements were acquired in the pattern shown with the scan point circled as the starting point. Arrows indicate the walking path for the instrument operator (Zhao et al., 2011).

within the Northern Experimental Forest of the International Paper CO., about 35 miles north of Bangor, Maine. It was established by the University of Maine. With coverage of about 7000 ha, the site contains an assortment of small plantations, multi-generation clearings, and large natural forest stands. The natural stands in this boreal-northern hardwood transitional forest are mixed, with hemlock (*Tsuga*), spruce (*Picea*), fir (*Abies*), aspen (*Populus*) and birch (*Betul*) species. The region has relatively little topographic relief, but soil drainage classes vary greatly over short distances (Kimes et al., 2006).

3.2. Field measurements

During the 2007 summer field campaign, ground-based vegetation structure data were collected in the three forest sites in New England (Strahler et al., 2011). Two stands were selected for each site, in total six stands, named as Harvard Hardwood, Harvard Hemlock, Bartlett B2, Bartlett C2, Howland Tower, and Howland Shelterwood. Each stand includes five circular plots with a center plot and four corner plots 35.4 m away from the center (Fig. 2), labeled as center (CT), north east (NE), north west (NW), south east (SE) and south west (SW) respectively. The only exception is the tower stand in Howland, including only three plots (center (CT), north (NO) and south (SO)). The radius of the circular plot is 25 m for the Harvard hardwood stand, MA and 20 m for

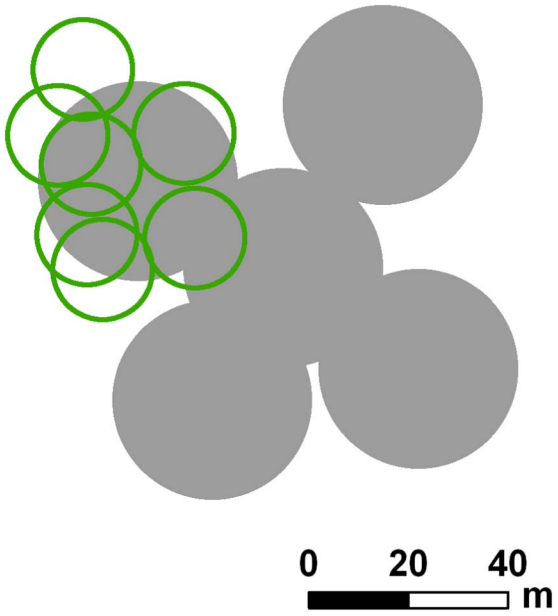

Fig. 4. Spatial sampling of LVIS over field plots (grey solid circles for the plot area and hollow circles for the estimated LVIS footprint. LVIS footprints with center within 5 m of plot range were selected for averaging. Note: Plot centers were taken as their observed GPS coordinates for the purpose of identifying overlapping LVIS footprints; the estimated position error of the centers is about ± 1.4 m.

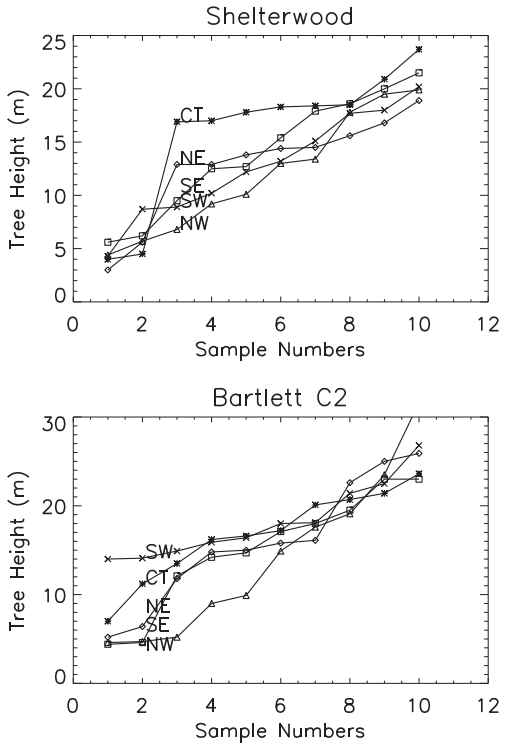

Fig. 5. Sampled tree height distributions for Howland Shelterwood and Bartlett C2. Shleterwood CT and NE plots, and Bartlett C2 SE and NE plots are treated as two-layer canopies.

the rest of the stands.

For all six stands, half were dominated by conifer trees and the other half by deciduous trees. The three conifer-dominated stands included one hemlock stand in the Harvard Forest, and two stands (Tower and Shelterwood) in the Howland Forest with hemlock, spruce, and white pine as dominant species. The deciduous-dominated stands included one hardwood stand in the Harvard Forest and both stands (B2 and C2)

Table 1
Input tree geometry parameters of the ACTS model for ten plots (CT, NE, NW, SE, SW) and the averaged for the whole stand(AVE) for two Harvard Forest stands.

Stand	Plot	R(m)	b(m)	λ(m^{-2})	h_1(m)	h_2(m)	REG-LAI	HAG-LAI	HEM-LAI	LIC-LAI
Harvard Hardwood	CT	1.81	5.49	0.073	11.70	20.14	4.42	5.41	4.03	4.58
	NE	2.70	4.38	0.066	8.06	22.53	4.55	5.95	3.40	4.73
	NW	1.78	4.21	0.066	5.31	20.14	4.76	5.47	3.13	4.69
	SE	1.71	4.32	0.070	9.81	21.01	4.30	4.38	3.30	3.99
	SW	1.99	5.37	0.063	6.32	21.86	5.02	5.65	3.47	3.86
	AVE	2.00	4.77	0.068	13.20	21.84	4.61			
Harvard Hemlock	CT	1.31	4.24	0.081	10.02	20.30	5.16	6.47	3.87	4.67
	NE	1.53	4.92	0.136	13.02	18.13	5.98	6.32	3.80	N/A
	NW	2.08	4.21	0.115	12.60	19.66	5.20	6.10	3.54	2.62
	SE	2.93	4.83	0.113	12.95	19.29	5.27	5.65	3.41	N/A
	SW	1.97	5.01	0.103	7.34	19.69	5.37	5.77	N/A	N/A
	AVE	1.76	4.43	0.109	7.68	18.60	5.40			

Table 2
Tree geometry inputs of the ACTS model for Bartlett and Howland Forests.

Stand	Plot	R(m)	b(m)	λ(m^{-2})	h_1(m)	h_2(m)	REG-LAI
Bartlett B2	CT	2.62	4.43	0.110	8.50	20.76	3.92
	NE	2.46	4.02	0.099	5.58	20.46	4.92
	NW	2.59	4.48	0.119	8.98	20.26	6.03
	SE	2.56	4.10	0.098	9.08	17.44	4.87
	SW	2.52	3.11	0.092	1.54	22.16	1.40
	AVE	2.57	4.10	0.103	4.04	21.07	4.92
Bartlett C2	CT	2.48	4.35	0.100	3.23	20.27	4.83
	NE_upper	2.93	6.83	0.053	15.85	19.48	2.00
	NE_under	3.09	3.09	0.039	9.06	12.55	2.83
	NW	5.11	3.28	0.094	3.50	21.59	5.72
	SE_upper	3.78	4.38	0.053	18.63	21.28	1.30
	SE_under	2.90	4.38	0.042	10.25	14.18	2.08
	SW	2.73	5.47	0.110	6.11	19.38	4.85
	AVE	2.76	4.35	0.098	1.49	20.76	4.72
Howland Tower	CT	1.74	2.93	0.222	3.29	14.58	5.49
	NO	1.55	4.67	0.210	6.14	15.95	5.84
	SO	1.57	2.48	0.220	6.87	15.92	4.69
	AVE	1.62	3.36	0.218	5.75	15.58	5.34
Howland Shelterwood	CT upper	2.95	6.05	0.051	7.09	17.85	3.04
	CT under	1.43	1.63	0.013	2.33	3.69	0.76
	NE upper	2.46	4.02	0.044	8.10	15.70	2.26
	NE under	1.24	1.53	0.011	1.68	6.61	0.57
	NW	2.20	3.74	0.071	3.97	16.79	6.03
	SE	1.23	4.43	0.073	5.85	16.96	2.88
	SW	1.96	4.20	0.061	5.18	15.59	4.55
	AVE	2.05	4.20	0.064	6.98	16.38	3.74

in Bartlett Forest with, dominant species of red oak, red maple, beech, birch and white ash. The stands/sites were selected to include different types of mixed growth forests, and a shelterwood partly harvested example.

In each plot, the number of trees was counted, excluding small trees with DBH < 3 cm. LAI were measured for each plot. Within each plot 10 trees were selected by systematic sampling, and tree size (horizontal and vertical crown radii, *R* and *b*) and tree height were measured (see Yao et al., 2011a, 2011b for details).

LAI was measured with three instruments: the Echidna® ground-based lidar, digital hemispherical photography, and LAI-2000 (see Zhao et al., 2011 for details). The ground-based lidar provides two LAI measurements: HAG-LAI based on the hinge angle (Warren-Wilson, 1963), and REG-LAI from regression of multiple angles measurements (Jupp et al., 2009). The hinge angle method uses gap probability with range in a band of zenith angles from 55° to 60°, where the effects of leaf angle distribution are minimized. That is, the projected leaf areas for common leaf angle distribution functions taken with zenith angle tend to converge at the zenith angle of $\tan^{-1}(\pi/2) = 57.5°$ ("hinge" angle), thus providing a view zenith angle that minimizes the effects of leaf angle distribution (Warren-Wilson, 1963). The regression method (Jupp et al., 2009) uses measurements of gap probability with range

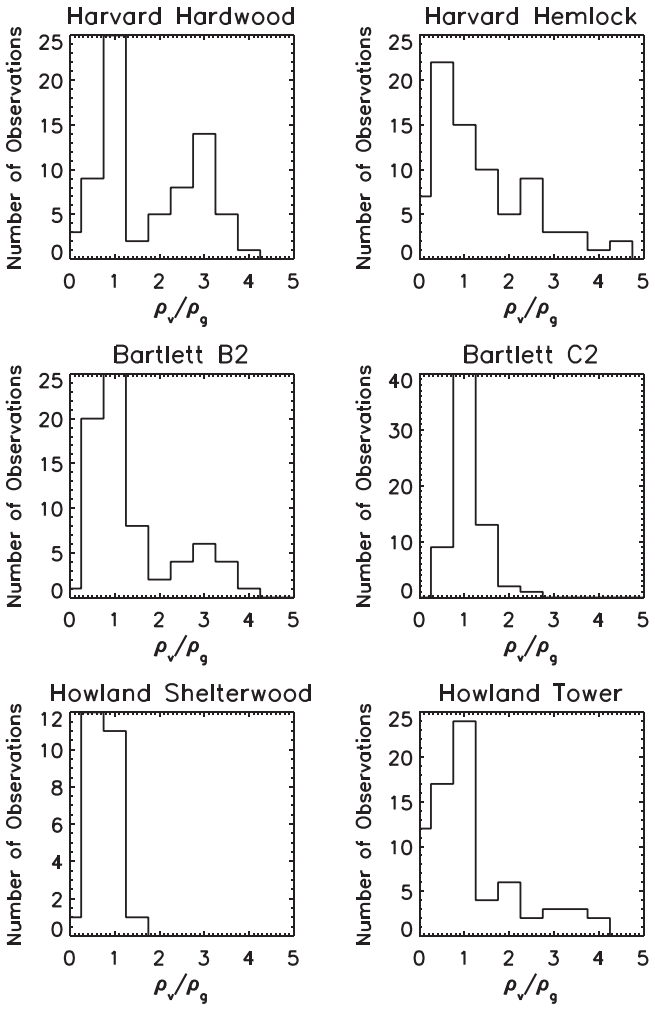

Fig. 6. Histogram of ρ_v/ρ_g extracted from LVIS data using Eq. (11) for the six study sites.

averaged in 12 zenith angle rings from 5–65° and is therefore likely to be more accurate.

LAI was also estimated based on gap probability extracted from hemispherical photographs (HEM-LAI). The hemispherical canopy photograph provides a commonly-used, indirect optical method to obtain leaf area index and canopy transmittance based on gap fractions derived from light attenuation within the canopy as measured by the contrast between sky and canopy elements (Hale and Edwards, 2002). In this study, a Nikon Coolpix 900 camera with a 180° fisheye lens pointed toward the zenith was used at a resolution of 1391 × 1405. All photographs were taken before sunrise or after sunset under clear sky

Table 3
Canopy and background reflectivity ratios in different forest stands used for the Radiation transfer Model Inter-comparison -IV (Widlowski et al., 2015).

Species, location	ρ_v/ρ_g
Pine, Estonia	0.78
Birch, Estonia	0.74
Maple, Estonia	0.82
Birch, Estonia	0.84
Alder, Estonia	0.88
Ash, Estonia	0.93
Linden, Estonia	0.79
Norway spruce, Estonia	0.77
Aspen, Estonia	0.76
Citrus orchard, South Africa	1.06
Short rotation forest, Italy	1.00

conditions to ensure homogeneous, shadow-free illumination of the canopy and high contrast in the blue spectral region between the canopy and the sky. To properly sample the spatial variability over the site, 13 hemispherical photographs were taken at a spacing of 10 m at each plot following the sample design in Fig. 3. All digital photographs were collected as highest-quality JPEG images and were analyzed using HemiView software (Dynamax, Inc., Houston, TX).

The LAI-2000 instrument was also used to measure effective LAI including clumping (Stenberg, 1996; Barclay and Trofymow, 2000) following the same observation plan as hemispherical canopy photographs (Fig. 3) (LIC-LAI). The LAI-2000 Plant Canopy Analyzer (Li-Cor Inc., 1992) is a portable instrument that provides LAI estimates by measuring radiation received by a fish-eye optical sensor in five zenith angle ranges under a forest canopy and comparing them to reference measurements of skylight collected simultaneously or contemporaneously in a nearby open area. The LAI-2000 instrument determines canopy light interception in five zenith bands centered at angles of 7°, 23°, 38°, 53°, and 68°. LAI is then estimated by inversion of measured light interception formulae. LAI-2000 LAI is effective LAI, which contains non-leaf area and includes the effects of clumping. All the LAI values compensate for some effects of clumping, therefore, all the LAI values were used as effective LAI in this study.

3.3. LVIS data

The LVIS is an airborne laser altimeter system designed to collect data on surface topography and vegetation structure (Blair et al., 1999). The onboard laser generates Gaussian shaped optical pulses at a wavelength of 1064 nm. The vertical sampling resolution of LVIS is 30 cm (1 ns) (Blair et al., 2004). LVIS footprint sizes (diameter) typically vary between 10 and 25 m depending on the mission flight altitude. The LVIS waveform continuously records the returned laser energy from the canopy surface with height within the footprint, resulting in complete vertical distribution of vegetation scattering profile (Blair et al., 1999).

In the summer of 2003, LVIS flew over some intensively studied forest sites in New England (Blair et al., 2004). The LVIS data used in this study were acquired on July 18–20, 2003 in Bartlett, NH, July 26, 2003 in Howland, ME, and July 20, 2003 in Harvard, MA. The field vegetation structure data used to drive our model was collected in 2007, and thus there is a four-year gap between LVIS data and field data. Any changes of vegetation structure within this period (vegetation growth, cutting) could cause mismatches between LVIS and model results, which can be quite pronounced in sparse canopies (see more detailed discussion in Section 5).

The LVIS footprint spacing over these sites was contiguous; the center of each footprint was separated by roughly 20 m with a 25 m footprint both across and along the flight path. LVIS samples were overlaid with one field plot (Fig. 4). LVIS sampling density for all the plots ranges from 3 to 19 (The exact sampling numbers for each plot can be found in Figs. 10 and 11).

Waveforms are digitized laser energy returns, i.e. the intensity, or the magnitude, of the return pulse at each canopy height level. In this study, the original LVIS waveforms were normalized by the total laser energy return to reflect the relative laser energy intensity at each height.

To extract LVIS data for the corresponding plots, we first selected the LVIS data with footprint centers located within a 5 m radius circle for each plot, then averaged these LVIS data, so that the selected LVIS observations can occupy an area slightly larger than plot range to reduce geolocation uncertainty (Ni-Meister et al., 2010a, 2010b).

Foliage profiles can be averaged arithmetically. However, as laser pulse has an exponential decay when penetrating into canopies, the best waveform averaging method is by geometric mean. Therefore, we used the geometric mean to average for plots and stands in this study.

4. Model inputs

Based on the field measurements, two sets of ACTS inputs were calculated: one at the plot level (a 20 or 25 m-radius circle) and the other at the stand level (1 ha area). The inputs include canopy layer status and tree density, tree shape (ellipsoidal) and size (horizontal and vertical crown radii), foliage area volume density, and leaf and background spectral reflectivity for each canopy layer.

Canopy layer status was obtained based on the individual tree height histogram (Fig. 5). If the tree height histogram shows a bimodal pattern, then the canopy of the plot is regarded as two-layer, otherwise, it is regarded as one-layer. Fig. 5 shows how Bartlett C2 NE and SE and Howland Shelterwood CT and NE were identified as two-layer canopies based on tree height distribution. Shelterwood CT and NE plots have two distinct layers. Bartlett C2 SE plot has two distinct tall trees, separated from the other trees underneath. Two smaller trees (< 5 m) could also be separated from the middle layer. Though it could be separated as a three-layer canopy in this case, we considered it as a two-

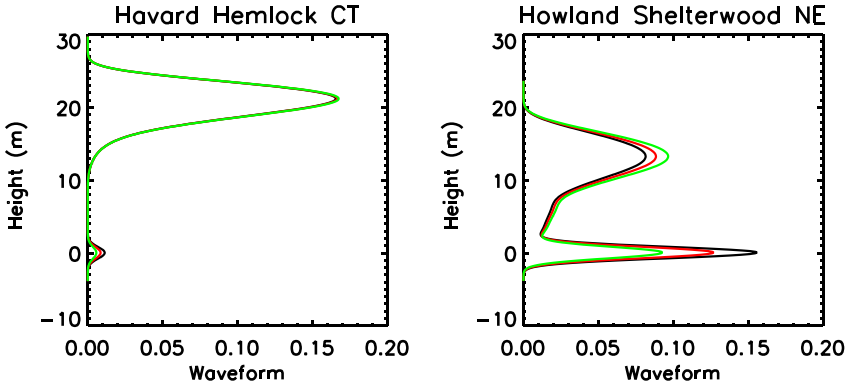

Fig. 7. The impact of ρ_v/ρ_g for dense and sparse canopies on simulated waveforms, the curves in black, red and green represent value as 0.75, 1.0 and 1.50 respectively. (For interpretation of the references to color in this figure legend, the reader is referred to the web version of this article.)

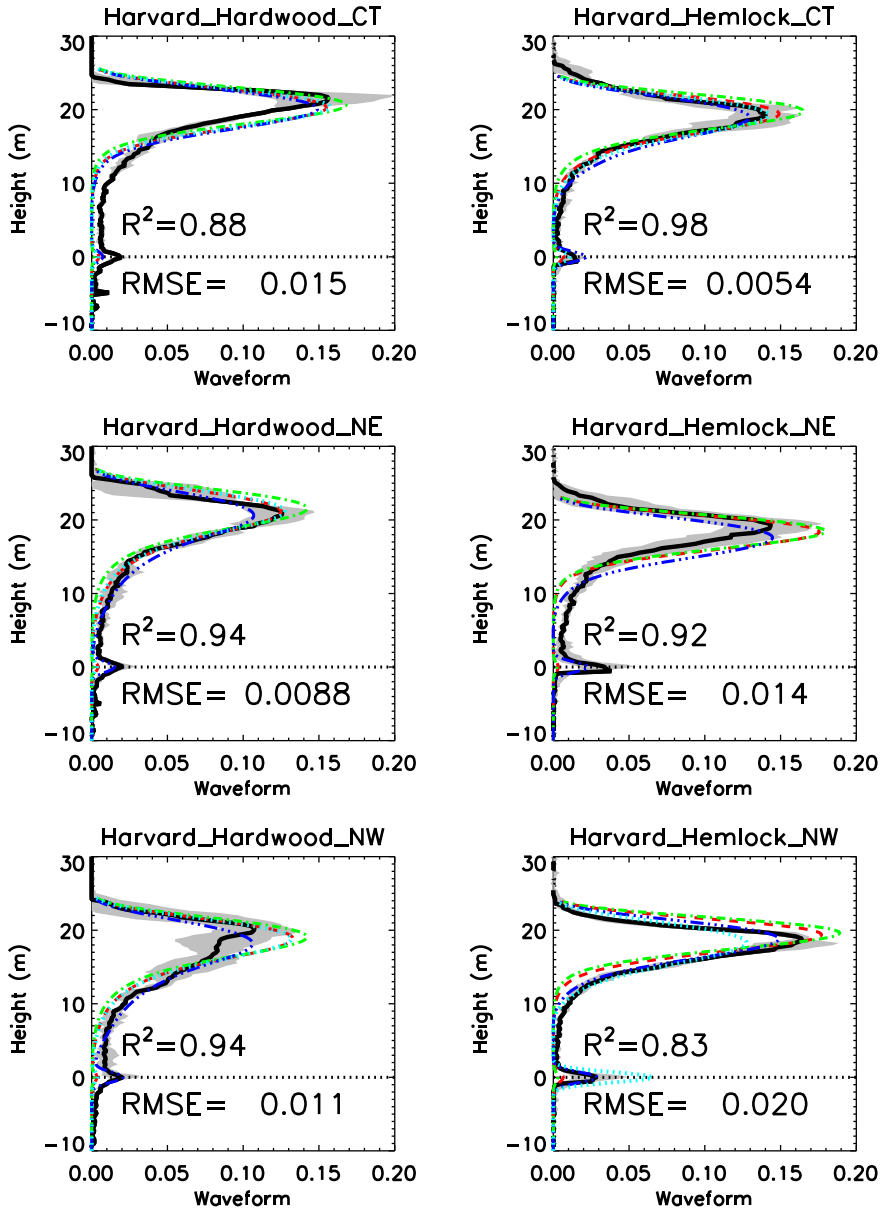

Fig. 8. Comparison of modeled waveforms and LVIS measurements (solid black) with shaded grey for standard deviation in different plots in a deciduous stand and a coniferous stand in Harvard Forest, MA (only six plots are included to show more detail comparison). In the modeled waveforms, four kinds of LAI values are used: REG-LAI (red, dash), HEM-LAI (blue, dash-dot-dot), HAG-LAI (green, dash-dot) and LIC-LAI (cyan, dot). Only showing the R^2 and RMSE values using REG-LAI. (For interpretation of the references to color in this figure legend, the reader is referred to the web version of this article.)

layer canopy due to limited tree sampling (10 per plot). The C2 NE plot shows three top trees distinguished from the rest, and it also could be taken as a three-layer canopy. Some other plots may show large variation of tree heights, however there is no clear distinction of layering and thus they were treated as one layer canopies. Some may have one tall tree distinguished from the rest and were also as one-layer canopies due to limited sampling.

4.1. Vegetation structure inputs

The input canopy geometry parameters for each layer were compiled based on the field canopy geometry data collected in 2007. These parameters include horizontal crown radius R, vertical crown radius b, stem count density λ, mean and standard deviation of crown center height, h_c, $mean(h_c)$ and $std(h_c)$ and the lower and upper bounds of canopy height, h_1 and h_2, calculated as $h_1 = mean(h_c) - std(h_c)$ and $h_2 = mean(h_c) + std(h_c)$. However due to limited sampling of ground data, in some cases h_1 and h_2 were adjusted to make sure that modeled waveform extent $(h_2 - h_1 + 2b)$ matches the LVIS waveform extent.

As discussed in Section 3.2, four kinds of LAI values were used in this study: two from the Echidna® ground-based lidar: HAG-LAI based on the hinge angle and REG-LAI from regression of multiple angles ground lidar measurements one from digital hemispherical photography (HEM-LAI), and one from LAI-2000 (LIC-LAI). Harvard Hardwood and Harvard Hemlock plots used all four sets of LAI values, while other plots used REG-LAI only. Table 1 lists the vegetation structure inputs for all plots and averaged for the whole stand in Harvard Forest, Table 2 for Bartlett and Howland Forests.

4.2. Spectral inputs

The spectral input for our model is the canopy and background reflectivity ratio, ρ_v/ρ_g, parameterized based on leaf single scattering albedo, leaf scattering phase function, and background albedo measurements. For a randomly-oriented leaf canopy, the ratio is a function of leaf reflectance and background albedo (Eq. (10)). We do not have site-specific background albedo and species-specific leaf reflectance measurements for our study sites. Because the background albedo ρ_g varies from site to site and leaf reflectance also depends on species, these measurements are not easy to acquire. The ratio is approximated

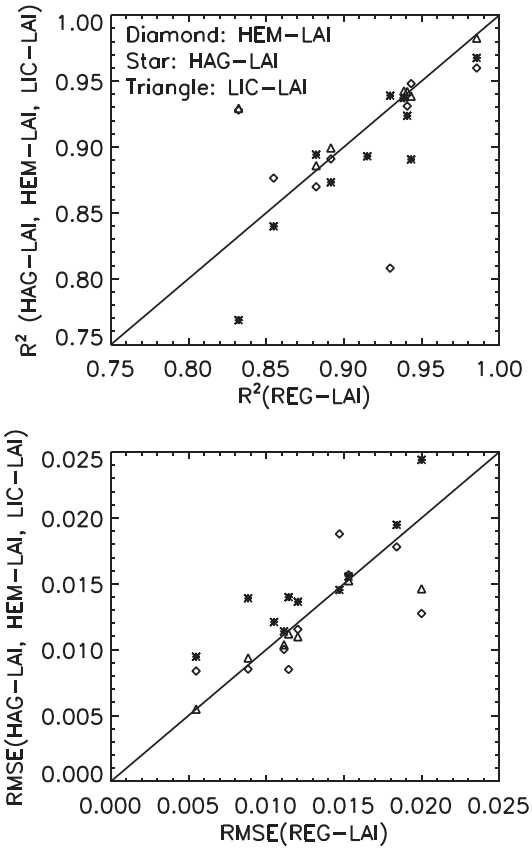

Fig. 9. Comparison of coefficients of determination (R^2) and RMSE of the modeled waveforms using REG-LAI (x-axis), HAG-LAI (y-axis, stars), HEM-LAI (y-axis, diamonds), and LIC-LAI (y-axis, triangles) for all 10 plots.

as unity (1) in this study based on the analysis from two different approaches as discussed below.

Ni-Meister et al. (2010a, 2010b) proposed an approach to estimate ρ_v/ρ_g from two adjacent lidar waveforms:

$$\rho_v/\rho_g = (R_{v1} - R_{v2})/(R_{g2} - R_{g1}) \quad (12)$$

where R_v and R_g are defined as the accumulated laser returns from the canopy and from the ground in each footprint, respectively; R_{v1}, R_{v2} and R_{g1}, R_{g2}, are the accumulated laser returns from canopy and background from two adjacent lidar waveforms.

Using LVIS data in each site, ρ_v/ρ_g was calculated based on Eq. (12), and Fig. 6 shows the histogram of ρ_v/ρ_g calculated over the six stands. The ratios are mainly centered at one for all stands except for the two conifer stands: Harvard Hemlock and Howland Shelterwood. Here the ratios show a slightly higher probability of being less than one. The bimodal feature at Harvard Hardwood stand may display the different vegetation optical properties of the dominant species, oak and birch, given the same ground optical properties.

It is rather difficult to quantitatively evaluate the accuracy of these values. To estimate if these values were in the right range, we used available field measurements of leaf single scattering albedo and background albedo measurements at 1064 nm wavelength for other sites as reference values. We chose to use field data collected in four forest stands acquired for the Radiation transfer Model Intercomparison IV (RAMI-IV and the web link: http://rami-benchmark.jrc.ec.europa.eu/HTML/RAMI-IV/RAMI-IV.php) exercise: a 124 year-old pine (*Pinus sylvestris*) stand in Jarvselja, Estonia; a 49 year-old birch (*Betula pendula*) stand in Jarvselja, Estonia; a 9 year-old citrus orchard in Wellington, South Africa; and a Lombardy short rotation forest of poplar clones in Parco Ticino, Italy. Table 3 lists the values of the ratios for different species in the above four stands. The ratio ranges from 0.77 to 1.05 over all the species across the three different countries. Conifer species show slightly lower ratios (0.77 and 0.78) than the deciduous species (most values larger than 0.9).

Overall, the values of the ratio calculated using Eq. (12) are similar to the values calculated based on Eq. (11) in Table 3. To simplify the modeling work, this study approximates the ratio as one. However using specific ratio values derived from Eq. (12) will improve the model result. Further, our comparison indicates that setting the ratio equal to one is to be generally acceptable for general purpose at this wavelength.

To evaluate the uncertainty of modeled waveforms with a simple ratio of one, we compared the modeled waveforms using three different ρ_v/ρ_g values (0.75, 1, and 1.25) for Harvard Hemlock, a relatively denser stand with very low ground returns in waveforms and Howland Shelterwood, a sparse stand with strong ground returns in waveforms (Fig. 7). For dense forest, different ratios from 0.75–1.25 result in very little differences in the modeled waveforms. However, for sparse stands, canopy peaks and the ground returns show quite large differences. A larger ratio leads to larger canopy peak returns and weaker ground returns and vice versa. This result suggests that lidar waveforms are sensitive to the canopy and background reflective ratio for sparse canopies. An overestimated ratio often leads to overestimated canopy peak returns and underestimated ground returns.

5. Results

5.1. Impact of different LAIs on modeled waveforms

To test the qualities of the four LAI measurements, we ran ACTS with four different LAI measurements as inputs for the ten plots of two Harvard stands. The modeled lidar waveforms were compared with LVIS measurements. Fig. 8 only includes the results from six plots (three from the Hardwood stand and three from the Hemlock stand). All the LAI measurements were treated as a clumped LAI- effective LAI based on the nature of the measurement itself (see discussion in Section 3.2). The modeled and LVIS waveforms are fairly similar using the four different LAI inputs. Fig. 8 shows the coefficient of determination (R^2) and Root-Mean-Square-Error (RMSE) using REG-LAI. The best performance has R^2 = 0.98 and RMSE = 0.0054. The worst one R^2 = 0.83 and RMSE = 0.02. Fig. 9 compares the model performance using all LAIs. In general, R^2 ranges from 0.77–0.98, and RMSE 0.005–0.025. Overall most R^2 and RMSE values are scattered around the 1:1 line. The worst RMSEs (R^2 = 0.76, and RMSE = 0.025 using HAG-LAI) are caused due to the misaligned waveforms in the Harvard Hemlock-NW plot. Overall, the modeled waveforms using four different LAI inputs are within the range of ± one standard deviation range of LVIS waveforms except for Havard Hemlock-NW.

To avoid the confusion of using too many LAI inputs for the model, only REG- LAI was used to drive ACTS in the following model simulations. Modeled waveforms were compared to LVIS data at two different scales: first at the 20 m-radius circular plot level and then at each stand (1-ha level).

5.2. Model and LVIS waveform comparison – plot scale

5.2.1. Bartlett experimental forest, NH

Fig. 10 compares both the modeled and LVIS waveforms for all plots at the Bartlett B2 and C2 stands. All five plots in Bartlett B2 were run with one-layer canopy. But NE and SE plots in Bartlett C2 were in two stories. Instead of plotting the mean and standard deviation of LVIS waveforms, Fig. 10 includes the mean and individual LVIS waveforms to show the complex vegetation structure characteristics.

Both observed and modeled waveforms show strong canopy returns and weak ground returns, indicating the Bartlett Forest is a dense forest (Schull et al., 2007). R^2 for all 10 plots ranges between 0.74 and 0.98 with RMSE between 0.006 and 0.014. The Bartlett C2 NE and SE plots are two-layer canopies. The model simulates the two expected peaks as

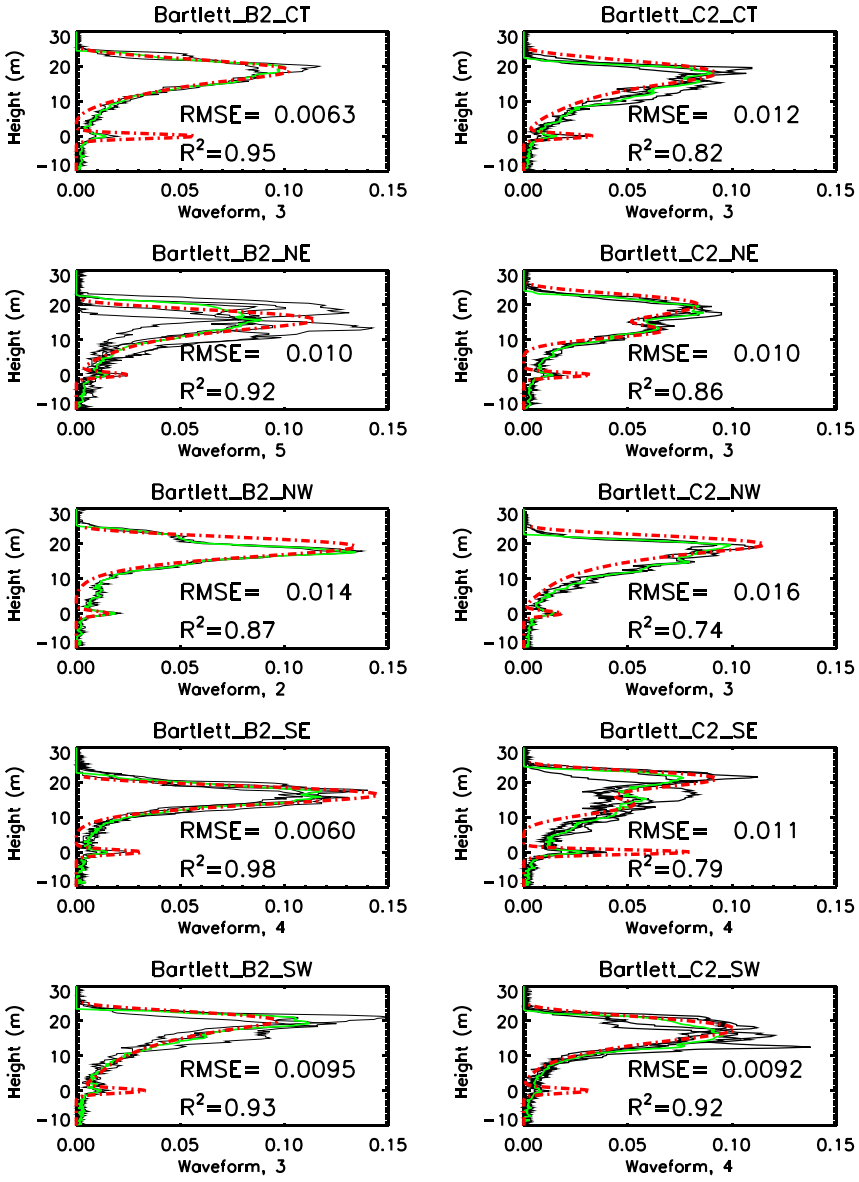

Fig. 10. Comparison of modeled waveforms (red) and individual LVIS measurements (black) and their geometric means (green) at different plots for the B2 and C2 stands in Bartlett, NH. (For interpretation of the references to color in this figure legend, the reader is referred to the web version of this article.)

shown in the averaged LVIS waveforms.

Some plots show mismatches between the modeled and LVIS waveforms. The Bartlett C2–NW plot has the largest RMSE = 0.016 and least R^2 = 0.74. For Bartlett C2 SE and NE plots, LVIS waveforms show stronger understory and ground returns. Bartlett C2 SE (R^2 = 0.79, RMSE = 0.01) has two distinct LVIS waveforms, indicating it is a complex plot. Even the two-layer model does not catch all the complex structure features without considering the impact of understory. As indicated by tree height measurements in Fig. 5, ideally these plots should be parameterized as three layer canopies; ignoring understory in the model results in weaker returns from the understory and stronger ground returns. A three-layer canopy model might work better here. However, due to the sparse samples of tree parameters, it was maintained as a two-layer canopy.

In addition, the modeled waveforms tend to slightly overestimate ground peak energy returns of LVIS measurements for all Bartlett plots. Using a canopy and ground reflectivity ratio of one may also contribute to the discrepancy. Bartlett is a deciduous forest and the ratio is likely larger than one as discussed before.

5.2.2. Forest ecosystem research site in Howland, ME

We compared the modeled waveforms with LVIS data for the three plots in the Howland Tower site and five plots in Shelterwood site (Fig. 11). Shelterwood CT and NE plots were treated as two-layer canopies, and the rest of the plots as one-layer canopies. For the three Howland Tower plots, the modeled waveforms are closely related to averaged LVIS waveforms with R^2 = 0.92–0.96 and RMSE = 0.06–0.01. However, results from the Shelterwood stand tell a different story. LVIS waveforms for all five plots show stronger ground returns indicating they were very sparse canopies in 2003 due to prior selective logging. After four years of growth, the modeled waveforms show much weaker ground returns and relatively stronger vegetation returns, indicating vegetation grew denser in 2007. Four plots have R^2 = 0.51–0.86 and RMSE = 0.024–0.026 and the worst plot R^2 = 0.29 and RMSE = 0.035. Discrepancy in modeled and LVIS waveforms suggest vegetation growth from 2003 to 2007 in the Shelterwood stand was significant. For other stands, where trees were dense, however, the growth in vegetation in this four-year period does not serve as an important factor causing the differences in modeled and LVIS waveforms.

5.3. Model and LVIS waveform comparison – stand scale

The modeled waveforms at stand level were also compared with

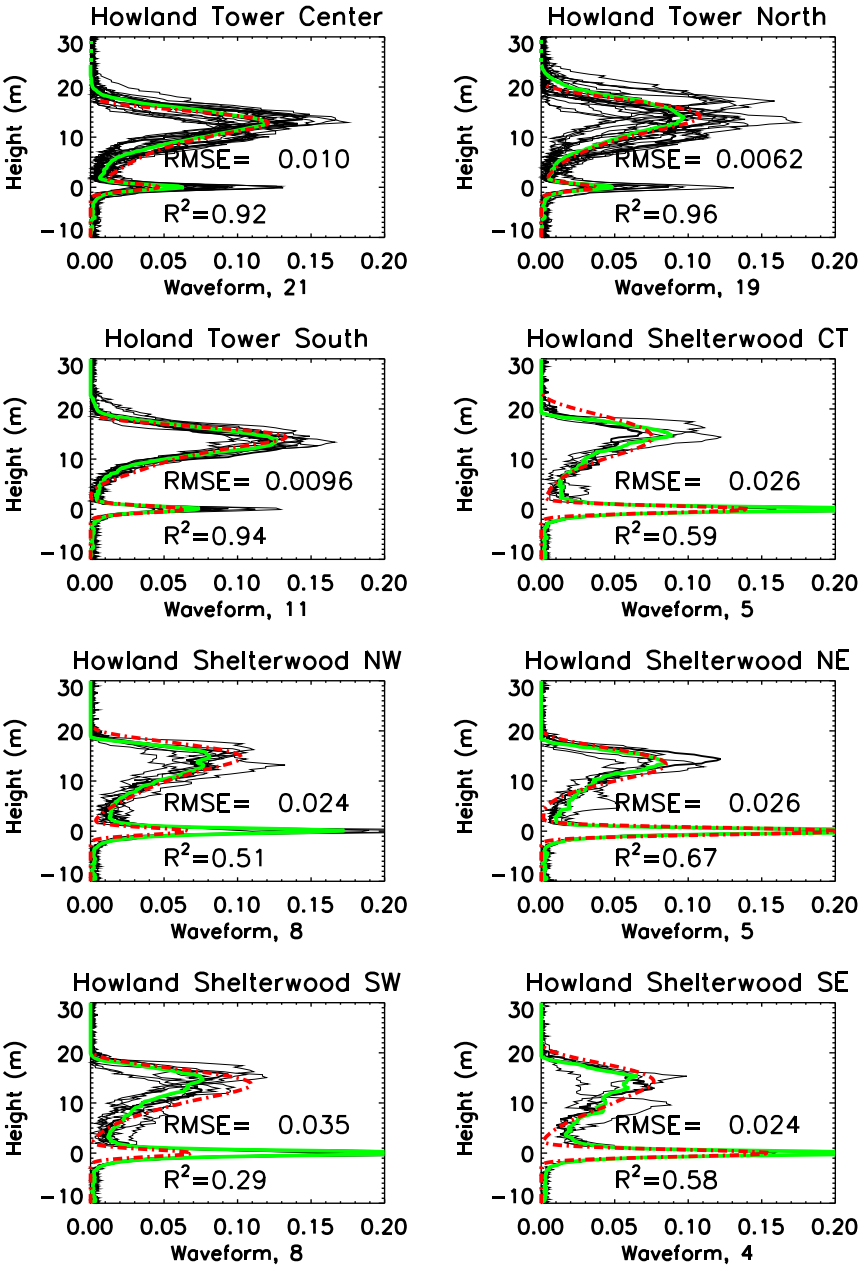

Fig. 11. Comparison of modeled waveforms (red) and individual LVIS measurements and their geometric means (green) at Howland Tower and Shelterwood. (For interpretation of the references to color in this figure legend, the reader is referred to the web version of this article.)

averaged LVIS waveforms at the six forest stands (100 m × 100 m) (Fig. 12). Model inputs at stand level were calculated using all the tree structure measurements collected for each stand. All stands were treated as one-layer canopies, as it is hard to distinguish different layers in tree height measurements for all plots in each stand.

Harvard Hardwood and Harvard Hemlock are quite dense forest stands with very small ground returns in both modeled and LVIS waveforms. R^2 = 0.92–0.94, RMSE = 0.01.

Bartlett B2 and Bartlett C2 are also relatively dense stands. R^2 = 0.86 (C2) and 0.90 (B2) and RMSE ~ 0.01. For the Bartlett C2 stand, the modeled waveform shows one strong canopy peak return at 20 m height level, while LVIS waveforms extend the canopy peak returns between 12 m–22 m height level, thus indicating that C2 stand has a more complex vegetation structure. As discussed before, C2 NE and SE plots are multilayer canopies; a one layer canopy model underrepresents the vertical variation of vegetation structure. A two-layer model might be required to correctly model lidar waveforms here. In addition, the model slightly overestimates the ground returns for Bartlett B2 and C2 stands. That may be due to the use of an underestimated canopy and background reflectance ratio in the model (see detailed discussion in previous section).

The Howland Tower and Shelterwood stands are relatively sparser canopies compared to the other four stands, particularly the Shelterwood stand. The model performs better in the Tower site than the Shelterwood site, with R^2 = 0.92 and RMSE = 0.012. For the Shelterwood stand, R^2 = 0.57 and RMSE = 0.028. The modeled waveform has stronger peak vegetation returns and weaker ground returns. The discrepancy can be attributed to four-year time difference in field and LVIS data collection timing, as discussed in Section 5.2.2.

5.4. Comparison between stand and plot scales

Fig. 13 compares the R^2 and RMSE at the stand (stars) and the plot (diamonds) scale for the six stands. Four stands–two Harvard stands, Bartlett B2 and Howland Tower, have R^2 > 0.90. For the Bartlett C2 stand R^2 is lower, around 0.86. The RMSE values are around 0.01 for all

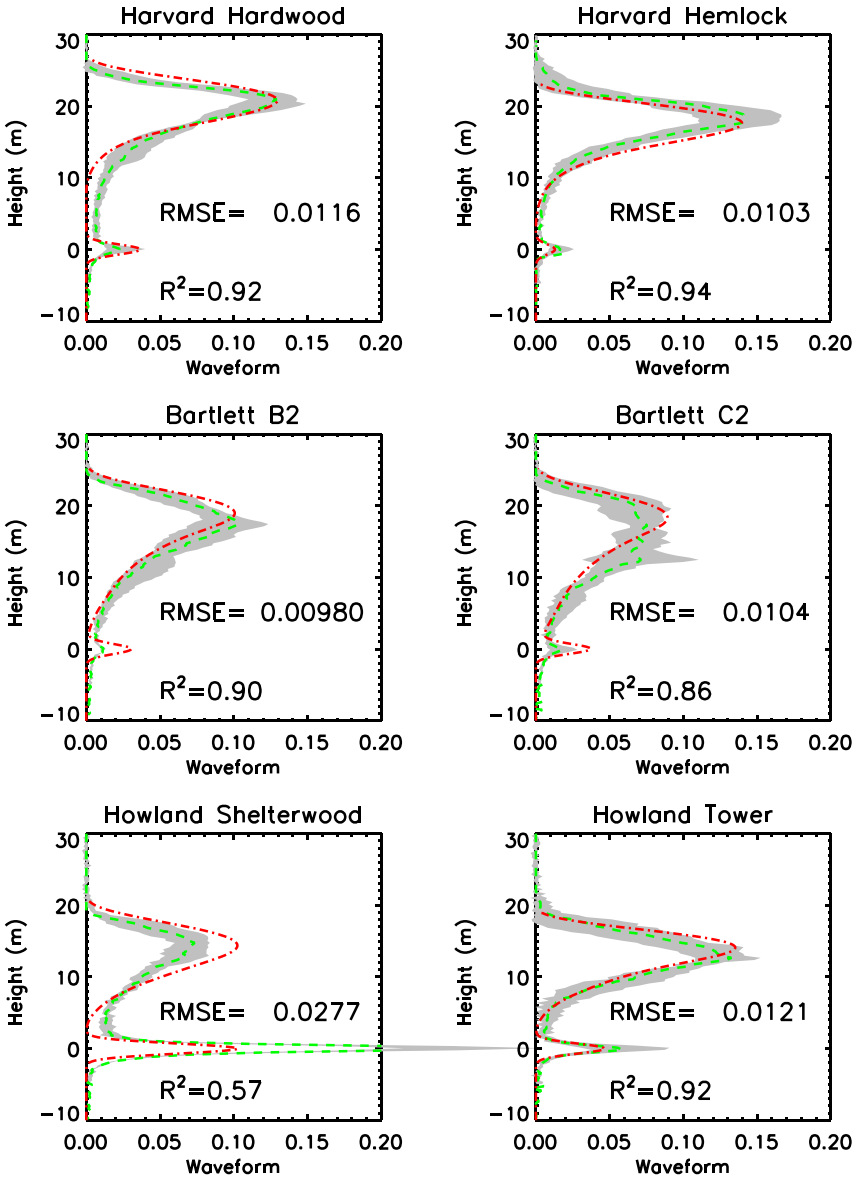

Fig. 12. Comparison of modeled waveforms (red) and LVIS measurements with shaded grey for standard deviation and green for the geometric means for six forest stands across the New England region. (For interpretation of the references to color in this figure legend, the reader is referred to the web version of this article.)

stands except for the Shelterwood stand. The Shelterwood stand has the lowest R^2 = 0.57 and largest RMSE = 0.028. The low performance for this stand is due to vegetation growth.

At the plot scale the model has similar performance as at the stand level, but with some variations, which is expected. Some plots perform better than the stand level, and some are worse. R^2 and RMSE vary around the corresponding value at the stand level. Howland Tower and Harvard Hardwood stands have smallest variation of plot level R^2,0.03, and 0.06 respectively, then Bartlett B2, 0.12, Harvard Hemlock, 0.16, Bartlett C2,0.17 respectively, and Shleterwood, the largest, 0.33.

The plot level RMSE has similar patterns as R^2. The plot level RMSE variations are different at different stands. Howland Tower has the lowest variation of plot level RMSE, (0.001). Harvard Hardwood (0.006), Bartlett B2 (0.008), and Bartlett C2 (0.007) have similar variations. Howland Shelterwood (0.01) and Harvard Hemlock (0.015) have the largest RMSE ranges, and the later has plot level RMSE variations larger than stand level RMSE.

6. Dicussion and conclusions

The Analytical Clumped Two-Stream (ACTS) canopy radiative transfer model was used to model large-footprint lidar waveforms in six forest stands in New England with vegetation structure data collected in summer 2007 as inputs. The model results were compared to LVIS data collected in summer 2003 in this region.

In summary, at the stand level, the overall coefficient of determination between the modeled and LVIS waveforms are $R^2 > 0.90$ for two Harvard stands, the Bartlett B2 and Howland Tower stands, For the Bartlett C2 stand R^2 is lower, around 0.86. The Shelterwood stand has the lowest R^2 = 0.57. The RMSE values are around 0.01 except for the Shelterwood stand. A more detailed comparison at the plot and stand levels indicates that the model at the plot level has similar performance as at the stand level, with some variations. Some plots perform better than the stand level, and some are worse.

Overall the one-layer model works well in relatively uniform stands (Harvard Hardwood, Harvard Hemlock, Bartlett B2 and Howland Tower). The difference between the modeled and LVIS measured vertical vegetation structure for the Bartlett C2 stand indicates that a two-layer model is necessary to fully model the lidar waveforms. The ACTS model was tested in different vegetation types with various vegetation complexity: single layer vs multilayer, and dense vs sparse, conifer and deciduous forests at both stand and plot scales with good accuracy.

We made an effort to explore how the model performance compares to other canopy lidar models. More recent work by Gastellu-Etchegorry

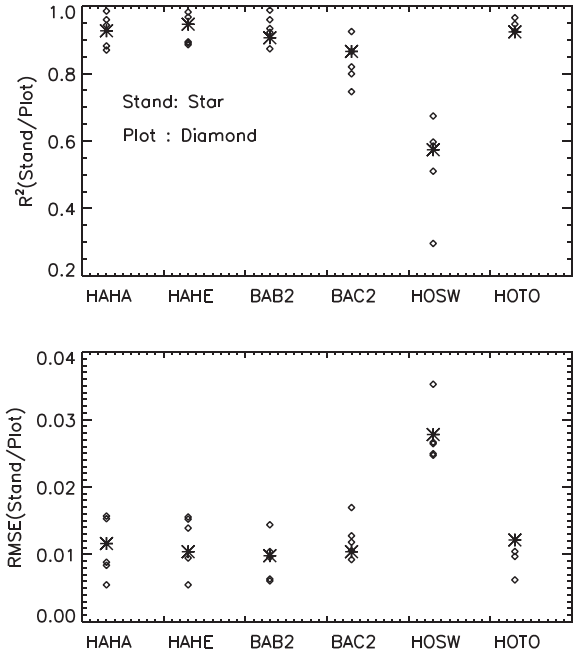

Fig. 13. Comparison of R^2 and RMSE at stand (stars) and plot (diamonds) levels for six stands: HAHA-Harvard Hardwood, HAHE-Harvard Hemlock, BAB2-Bartlett B2, BAC2-Bartlett C2, HOSH-Howland Shelterwood, HOTO-Howland Tower.

et al. (2016) compared the Discrete Anisotropic Radiative Transfer (DART) modeled and LVIS waveforms in Howland Tower site. The coefficients of determination (R^2) between the 89 pairs of LVIS and DART simulated waveforms range from 0.28 to 0.96, with a mean R^2 of 0.65 and a median R^2 of 0.70 and RMSE ranges from 0.0422 to 0.2092 for the selected waveforms. Rosette et al. (2013) used the same LVIS data to compare with the FLIGHT model (Rosette et al., 2013), however we could not identify a quantitative evaluation value. Compared to DART, ACTS has higher R^2 and lower RMSE values.

More importantly this quantitative error information could be valuable information for model inversion. Currently we are developing a Bayesian inversion approach to incorporate the impact of model uncertainty on model inversion accuracy.

The LVIS waveforms contain rich canopy structural information, which is valuable for ecological, hydrological and climate research. ACTS describes how canopy structure parameters are linked with LVIS waveform measurements based on the geometric optics and radiative transfer (GORT) theory. This study demonstrates that with field-measured vegetation structure inputs, ACTS can produce the complex features of lidar waveforms. This validation results demonstrate that ACTS has the capability to describe the physical nature of the relationship between lidar waveforms and vegetation structure.

7. Potential applications

7.1. Model inversion

This validation effort shed light on some potential applications of using ACTS in lidar research fields. First of all, ACTS offers a simple but physically-based model for inversion. Some single or lumped structure parameters can be analytically inverted to avoid the ill-posed inversion problem – possible multiple solutions from one set of measurements. ACTS can be used in inverse mode to retrieve canopy gap probability, foliage profile and specific structure information s such as crown size, density and foliage density. This structure information will be critical for understanding the terrestrial ecosystem functions, estimating global carbon budget, characterizing the impact of vegetation structure change on climate, habitat and biodiversity.

These 3D structure parameters can be directly used to initialize the structure inputs for structure-based dynamic terrestrial ecosystem modeling, such as Ent and ED for improved carbon flux and stock estimates to improve estimates of carbon stocks and fluxes, in forest management. Currently those model inputs are parameterized based on plant functional types and LAI derived from passive remote sensing data. Hurtt et al. (2004) showed that just lidar-based tree height measurements provided substantial constraints on model estimates of both carbon stocks and net carbon fluxes.

7.2. Forward model applications

Another application of this modeling effort is to better understand the underlying intrinsic nature of how each vegetation structure parameter contributes to waveforms. Understanding the intrinsic nature may aid us in exploring new approaches to retrieving parameter estimates from lidar measurements. For example, Ni-Meister and Lee (2016) were able to derive an analytical relationship between above-ground biomass and lidar waveforms based on a simplified ACTS model. Using the relationship, above-ground biomass can be directly derived from lidar waveform data. Our initial test results show that the analytical approach to retrieve above-ground biomass from waveforms outperforms the traditional height-metrics based above-ground biomass retrieval (see more detail in Ni-Meister and Lee, 2016. The model can also be applied to small footprint waveform and discrete lidar at stand/plot scales in different aspects. For example, Armston et al., 2013 uses the ACTS model and the method to retrieve ratio of canopy and background returns described in Ni-Meister et al. (2010b) to retrieve canopy gap probability from both full waveform and discrete lidar. Built on Armston et al. (2013), Chen et al. (2014) used an extension of ACTS described in Yang et al. (2011) to test the sensitivity of canopy gap probability to surface topography and survey characteristics. Ni-Meister et al. (2008) used the original GO-based model (Ni-Meister et al., 2001) to simulate canopy gap probability retrieved from a terrestrial lidar, Echidna Validation Instrument (EVI) (Strahler et al., 2008).

7.3. Sensor design

Lastly, the ACTS model can also be used to assess the sensitivities of waveforms to surface topography and off-nadir pointing effects, which will provide further valuable information on vegetation structure retrieval accuracies. Yang et al. (2011) expanded ACTS to study the impact of these effects on lidar waveform and vegetation height metrics retrieval. Both off-nadir pointing and surface topography stretch waveforms, which smears out the ground return. For large footprint lidar, such as ICESat-GLAS (65 m–90 m), surface topography has a big effect on lidar waveform and height metrics. Lee et al. (2011) used this model to correct the impact of surface topography on tree height retrieval from ICESat-GLAS data with success.

For medium footprint lidar, such as the GEDI instrument to be borne on the International Space Station, the off-nadir angle is about ± 5° (Ralph Dubayah - personal communication), for LVIS ± 6° (J. Bryan Blair – personal communication). Thus, the surface topography and off-nadir pointing effects are much weaker. Using the ACTS model, Yang et al. (2011) showed that a five-degree-off-nadir angle can lead to one meter overestimation on RH100. The impact on RH50 is much smaller than on RH100. The impact of five-degree-off-nadir pointing angle on waveforms varies with vegetation density. For a relatively dense forest, Yang et al. (2011) demonstrated the impact on peak vegetation returns is < 5%. The ACTS model has proven to be a valuable tool in predicting performance characteristics of a future sensor.

For small footprint lidar, due to its small footprint size, the impact of surface topography on waveforms is minimal. However, most small footprint lidar use large scan angles. For example, the Optech Galaxy sensor routinely operates with a 30° scan angle, and can range from 18°–42°. The Leica ALS50-II scans at 20° (Warne et al., 2009). Large

scan angles lead to extended waveforms and may have large impact on vegetation structure retrievals. ACTS can be used to study this impact.

With the evaluation presented in this study, the simple and analytical ACTS model was proven to be a useful tool to retrieve different vegetation structure parameters from large footprint lidar measurements. Its application is not only limited to large footprint lidar, but also extends to medium and small-footprint lidar.

Acknowledgements

The authors are greatly indebted to three reviewers for their thorough reviews of the manuscript, which helped us improve the quality of the manuscript significantly. The research undertaken for this paper was partially funded by NASA Grant NNX10AG28G.

References

Anderson, J.E., Martin, M.E., Smith, M.L., Dubayah, R.O., Hofton, M., Hyde, P., Peterson, B.E., Blair, J.B., Knox, R.G., 2006. The use of waveform Lidar to measure northern temperate mixed conifer and deciduous forest structure in New Hampshire. Remote Sens. Environ. 105 (3), 248–261.

Anderson, J.E., Plourde, L.C., Martin, M.E., Braswell, B.H., Smith, M.-L., Dubayah, R.O., Hofton, M.A., Blair, J.B., 2008. Integrating waveform Lidar with hyperspectral imagery for inventory of a northern temperate forest. Remote Sens. Environ. 112, 1856–1870.

Armston, J., Disney, M., Lewis, P., Scarth, P., Phinn, S., Lucas, R., Bunting, P., Goodwin, N., 2013. Direct retrieval of canopy gap probability using airborne waveform Lidar. Remote Sens. Environ. 134, 24–38.

Barclay, H.J., Trofymow, J.A., 2000. Relationship of readings from the Li-COR canopy analyzer to total one-sided leaf area index and stand structure in immature Douglas-fir. For. Ecol. Manag. 132 (2–3), 121–126.

Barford, C.C., Wofsy, S.C., Goulden, M.L., Munger, J.W., Hammond, E., Pyle, S.P., ... Moore, K., 2001. Factors controlling long- and short-term sequestration of atmospheric CO_2 in a mid-latitude forest. Science 294, 1688–1690.

Blair, J.B., Rabine, D.L., Hofton, M.A., 1999. The Laser Vegetation Imaging Sensor (LVIS): a medium-altitude, digitisation-only, airborne laser altimeter for mapping vegetation and topography. J. Photogramm. Remote Sens. 54, 115–122.

Blair, J.B., Hofton, M.A., Rabine, D.L., 2004. Processing of NASA LVIS Elevation and Canopy (LGE, LCE and LGW) Data Products, Version 1.0. http://lvis.gsfc.nasa.gov.

Bye, I.J., North, P.R.J., Los, S.O., Kljun, N., Rosette, J.A.B., Hopkinson, C., Chasmer, L., Mahoney, C., 2017. Estimating forest canopy parameter from satellite waveform Lidar by inversion of the FLIGHT three-dimensional radiative transfer model. Remote Sens. Environ. 188 (177–189).

Calders, K., Lewis, P., Disney, M.I., Verbesselt, J., Herold, M., 2013. Modelling Lidar waveforms to solve for canopy properties. Remote Sens. Environ. 134, 39–49. http://dx.doi.org/10.1016/j.rse.2013.02.018.

Chen, X.T., Disney, M.I., Lewis, P., Armston, J., Han, J.T., Li, J.C., 2014. Sensitivity of direct canopy gap fraction retrieval from airborne waveform Lidar to topography and survey characteristics. Remote Sens. Environ. 143, 25.

Disney, M.I., Kalogirou, V., Lewis, P.E., Prieto-Blanco, A., Hancock, S., Pfeifer, M., 2010. Simulating the impact of discrete-return lidar system and survey characteristics over 2 young conifer and broadleaf forests. Remote Sens. Environ. 114, 1546–1560. http://dx.doi.org/10.1016/j.rse.2010.02.009.

Drake, J.B., Dubayah, R.O., Clark, D.B., Knox, R.G., Blair, J.B., Hofton, M.A., Chazdon, R.L., Weishampel, J.F., Prince, S., 2002a. Estimation of tropical forest structural characteristics using large-footprint lidar. Remote Sens. Environ. 79, 305–319.

Drake, J.B., Dubayah, R.O., Knox, R.G., Clark, D.B., Blair, J.B., 2002b. Sensitivity of large-footprint Lidar to canopy structure and biomass in a neotropical rainforest. Remote Sens. Environ. 81, 378–392.

Drake, J.B., Knox, R.G., Dubayah, R.O., Clark, D.B., Condit, R., Blair, J.B., Hofton, M., 2003. Above-ground biomass estimation in closed canopy Neotropical forests using Lidar remote sensing: factors affecting the generality of relationships. Glob. Ecol. Biogeogr. 12, 147–159.

Dubayah, R.O., Drake, J.B., 2000. Lidar remote sensing for forestry. J. For. 98, 44–46.

Gastellu-Etchegorry, J.P., Yin, T., Lauret, N., Grau, E., Rubio, J., Cook, B.D., Morton, D.C., Sun, G., 2016. Simulation of satellite, airborne and terrestrial LiDAR with DART (I): waveform simulation with quasi-Monte Carlo ray tracing. Remote Sens. Environ. 184 (2016), 418–435.

Goetz, S., Steinberg, D., Dubayah, R., Blair, B., 2007. Laser remote sensing of canopy habitat heterogeneity as a predictor of bird species richness in an eastern temperate forest, USA. Remote Sens. Environ. 108, 254–263. http://dx.doi.org/10.1016/j.rse.2006.11.016.

Hale, S.E., Edwards, C., 2002. Comparison of film and digital hemispherical photography across a wide range of canopy densities. Agric. For. Meteorol. 112, 51–56.

Hancock, S., Lewis, P., Disney, M.I., Foster, M., Muller, J.-P., 2008. Assessing the Accuracy of Forest Height Estimation with Long Pulse Waveform Lidar Through Monte-Carlo Ray Tracing. Silvilaser, Edinburgh (September, 17–18).

Hancock, S., Armston, J., Li, Z., Gaulton, R., Lewis, P., Disney, M., Danson, F.M., Strahler, A., Schaaf, C., Anderson, K., Gaston, K.J., 2015. Remote Sens. Environ. 164, 208–224.

Hancock, S., Anderson, K., Disney, M., Gaston, K.J., 2017. Measurement of fine-spatial-resolution 3D vegetation structure with airborne waveform lidar: calibration and validation with voxelised terrestrial lidar. Remote Sens. Environ. 188, 37–50.

Harding, D.J., Carabajal, C.C., 2005. ICESat waveform measurements of within-footprint topographic relief and vegetation vertical structure. Geophys. Res. Lett. 32, L21S10. http://dx.doi.org/10.1029/2005GL023471.

Hurtt, G.C., Dubayah, R., Drake, J., Moorcroft, P.R., Pacala, S.W., Blair, J.B., Fearon, M.G., 2004. Beyond potential vegetation: combining lidar data and a height-structured model for carbon studies. Ecol. Appl. 14 (3), 873–883.

Jupp, D.L.B., Culvenor, D.S., Lovell, J.L., Newnham, G.J., Strahler, A.H., Woodcock, C.E., 2009. Estimating forest LAI profiles and structural parameters using a ground based laser called "Echidna®". Tree Physiol. 29 (2), 171–181.

Kiang, N.Y., Aleinov, I., Ni-Meister, W., Moorcroft, P.R., Koster, R.D., Kharecha, P., Kim, Y., Yang, W., Puma, M., 2008. The Ent dynamic global terrestrial ecosystem model (DGTEM) in the GISS GCM: algorithms for mixed vegetation communities. Geophys. Res. Abstr. 10, EGU2008–11418 (SRef-ID: 1607-7962/gra/EGU2008-A-11418 EGU General Assembly, Vienna, Austria, April 13–18, 2008).

Kimes, D.S., Ranson, K.J., Sun, G., Blair, J.B., 2006. Predicting Lidar measured forest vertical structure from multi-angle spectral data. Remote Sens. Environ. 100, 503–511.

Lee, S., Ni-Meister, W., Yang, W., 2011. Physically based vertical vegetation structure retrieval from ICESat data: validation using airborne data in White Mountain National Forest, New Hampshire, USA. Remote Sens. Environ. 115 (11), 2776–2785.

Lefsky, M.A., Cohen, W.B., Acker, S.A., Parker, G., Spies, T.A., Harding, D., 1999. Lidar remote sensing of the canopy structure and biophysical properties of Douglas Fir-Western Hemlock Forests. Remote Sens. Environ. 70, 339–361.

Lefsky, M.A., Cohen, W.B., Parker, G.G., Harding, D.J., 2002. Lidar remote sensing for ecosystem studies. Bioscience 52 (1), 19–30.

Lefsky, M.A., Harding, D.J., Keller, M., Cohen, W.B., Carabajal, C.C., Espirito-Santo, F.D., et al., 2005. Estimates of forest canopy height and aboveground biomass using ICESat. Geophys. Res. Lett. 32, L22S02.

Li, X., Strahler, A.H., Woodcock, C.E., 1995. A hybrid geometric optical-radiative transfer approach for modeling albedo and directional reflectance of discontinuous canopies. IEEE Trans. Geosci. Remote Sens. 33 (2), 466–480.

Moorcroft, P.R., Hurtt, G.C., Pacala, S.W., 2001. A method for scaling vegetation dynamics: the ecosystem demography model (ED). Ecol. Monogr. 71 (4), 557–585.

Ni-Meister, W., 2015. Aboveground terrestrial biomass and carbon stock estimations from multisensory remote sensing. In: Remote Sensing Handbook. CRC Press (ISBN-13: 978-1482218015, ISBN-10: 1482218011).

Ni-Meister, W., Lee, S., 2016. Allometric relationships between above-ground biomass and LiDAR full waveform measurements. Am. Geophys. Union (San Francisco, CA, December 14-18 (oral presentation)).

Ni-Meister, W., Jupp, D.L.B., Dubayah, R., 2001. Modeling Lidar waveforms in heterogeneous and discrete canopies. IEEE Trans. Geosci. Remote Sens. 39 (9), 1943–1958.

Ni-Meister, W., Strahler, A., Woodcock, C.E., Schaaf, C., Jupp, D.L.B., Yao, T., Zhao, F., Yang, X., 2008. Modeling the hemispherical scanning, below-canopy Lidar and vegetation structure characteristics with a geometric-optical and radiative-transfer model. Can. J. Remote. Sens. 34 (Suppl. 2), S385–S397.

Ni-Meister, W., Yang, W., Kiang, N., 2010a. A clumped-foliage canopy radiative transfer model for a global dynamic terrestrial ecosystem model I: theory. Agric. For. Meteorol. 150 (7–8), 881–894. http://dx.doi.org/10.1016/j.agrformet.2010.02.009.

Ni-Meister, W., Lee, S., Strahler, A.H., Woodcock, C.E., Schaaf, C., Ranson, J., Sun, G., Blair, J.B., 2010b. Assessing general relationships between above-ground biomass and vegetation structure parameters for improved carbon estimate from vegetation lidar. J. Geophys. Res. 115, G00E11. http://dx.doi.org/10.1029/2009JG000936.

North, P.R.J., Rosette, J.A., Suarez, J.C., Los, S.O., 2010. A Monte Carlo radiative transfer model of satellite waveform Lidar. Int. J. Remote Sens. 31 (5), 1343–1358.

Rosette, J.A.B., North, P.R.J., Suarez, J.C., 2008. Vegetation height estimates for a mixed temperate forest using satellite laser altimetry. Int. J. Remote Sens. 29, 1475–1493.

Rosette, J.A.B., North, P.R.J., Rubio-Gil, J., Cook, B., Los, S., Suarez, J., Sun, G., Ranson, J., Blair, B.J., 2013. Evaluating prospects for improved forest parameter retrieval from satellite Lidar using a physically-based radiative transfer model. IEEE Sel. Top. Appl. Earth Obs. Remote Sens. 6 (1), 45–53.

Schull, M.A., Ganguly, S., Samanta, A., Huang, D., Shabanov, N.V., Jenkins, J.P., Chiu, J.C., Marshak, A., Blair, J.B., Myneni, R.B., Knyazikhin, Y., 2007. Physical interpretation of the correlation between multi-angle spectral data and canopy height. Geophys. Res. Lett. 34, L18405. http://dx.doi.org/10.1029/2007GL031143.

Selkowitz, D.J., Green, G., Peterson, B., Wylie, B., 2012. A multi-sensor lidar, multispectral and multi-angular approach for mapping canopy height in boreal forest regions. Remote Sens. Environ. 121, 458–471.

Spies, T.A., 1998. Forest structure: a key to the ecosystem. Northwest Sci. 72, 34–39.

Stenberg, P., 1996. Correcting LAI-2000 estimates for the clumping of needles in shots of conifers. Agric. For. Meteorol. 79 (1–2), 1–8.

Strahler, A.H., Jupp, D.L.B., Woodcock, C.E., Schaaf, C.B., Yao, T., Zhao, F., et al., 2008. Retrieval of forest structure parameters using a ground-based lidar instrument (Echidna@). Can. J. Remote. Sens. 34 (Suppl. 2).

Strahler, A.H., Schaaf, C., Woodcock, C., Jupp, D., Culvenor, D., Newnham, G., Dubayah, R., Yao, T., Zhao, F., Yang, X., 2011. ECHIDNA Lidar Campaigns: Forest Canopy Imagery and Field Data, U.S.A., 2007–2009. ORNL DAAC, Oak Ridge, Tennessee, USA. http://dx.doi.org/10.3334/ORNLDAAC/1045.

Sun, G., Ranson, K.J., 2000. Modeling Lidar returns from forest canopies. A three-dimensional radar backscatter model of forest canopies. IEEE Trans. Geosci. Remote Sens. 38 (6), 2617–2626.

Tang, H., Dubayah, R., Swatantran, A., Hofton, M., Sheldon, S., Clark, D.B., et al., 2012. Retrieval of vertical LAI profiles over tropical rain forests using waveform lidar at LaSelva, Costa Rica. Remote Sens. Environ. 124, 242–250.

Tang, H., Brolly, M., Zhao, F., Strahler, A.H., Schaaf, C.L., Ganguly, S., et al., 2014.

Deriving and validating Leaf Area Index (LAI) at multiple spatial scales through lidar remote sensing: a case study in Sierra National Forest, CA. Remote Sens. Environ. 143, 131–141.

Warne, T.A., Nellis, M.D., Foody, G.M., 2009. The SAGE Handbook of Remote Sensing. SAGE Publications Ltd (ISBN-13: 978-1412936163, ISBN-10: 1412936160).

Warren-Wilson, J., 1963. Estimation of foliage denseness and foliage angle by inclined point quadrats. Aust. J. Bot. 11, 95–105.

Widlowski, J.L., Mio, C., Disney, M., Adams, J., Andredakis, I., Atzberger, C., Brennan, J., Busetto, L., Chelle, M., Ceccherini, G., Colombo, R., Côté, J.F., Eenmäe, A., Essery, R., GastelluEtchegorry, J.P., Gobron, N., Grau, E., Haverd, V., Homolová, L., Huang, H., Hunt, L., Kobayashi, H., Koetz, B., Kuusk, A., Kuusk, J., Lang, M., Lewis, P.E., Lovell, J.L., Malenovský, Z., Meroni, M., Morsdorf, F., Mõttus, M., NiMeister, W., Pinty, B., Rautiainen, M., Schlerf, M., Somers, B., Stuckens, J., Verstraete, M.M., Yang, W., Zhao, F., Zenone, T., 2015. The fourth phase of the radiative transfer model intercomparison (RAMI) exercise: actual canopy scenarios and conformity testing. Remote Sens. Environ. 169, 418–437.

Yang, W., Ni-Meister, W., Kiang, N., Moorcroft, P.R., Strahler, A.H., Oliphant, A., 2010. A clumped-foliage canopy radiative transfer model for a global dynamic terrestrial ecosystem model I: validation. Agric. For. Meteorol. 150 (7–8), 895907. http://dx.doi.org/10.1016/j.agrformet.2010.02.008.

Yang, W., Ni-Meister, W., Lee, S., 2011. Assessment of the impacts of surface topography, off-nadir pointing and vegetation structure on vegetation lidar waveforms using an extended geometric optical and radiative transfer model. Remote Sens. Environ. 115, 2810–2822.

Yao, T., Yang, X.Y., Zhao, F., Wang, Z.S., Zhang, Q.L., Jupp, D.L.B., Culvenor, D.S., Newnham, G.J., Ni-Meister, W., Schaaf, C.B., Woodcock, C.E., Strahler, A.H., 2011a. Measuring forest structure and biomass in New England forest stands using Echidna ground-based lidar. Remote Sens. Environ. 115, 2965–2974.

Yao, T., Yang, X., Gao, F., Wang, Z., Zhang, Q., Jupp, D., Culvenor, D., Newnham, G., Ni-Meister, W., Schaaf, C.B., Woodcock, C., Strahler, A., 2011b. Estimation of forest structure parameter and biomass New England forest stands using Echidna ground-based lidar. Remote Sens. Environ. 115 (11), 2965–2974.

Zhao, F., Yang, X.Y., Schull, M.A., Roman-Colon, M.O., Yao, T., Wang, Z.S., et al., 2011. Measuring effective leaf area index, foliage profile, and stand height in New England forest stands using a full-waveform ground-based lidar. Remote Sens. Environ. 115, 2954–2964.

Zwally, H.J., Schutz, B., Abdalati, W., Abshire, J., Bentley, C., Brenner, A., Bufton, J., Dezio, J., Hancock, D., Harding, D., Herring, T., Minster, B., Quinn, K., Palm, S., Spinhirne, J., Thomas, R., 2002. ICESat's laser measurements of polar ice, atmosphere, ocean and land. J. Geodyn. 34, 405–445.